



# Investigations of Flow Phenomena Over a Flat Plate and NACA0012 Airfoil at High Angles of Attack

Shailesh Kr Jha<sup>1</sup> · Uddipta Gautam<sup>1</sup> · Pramod Pawar<sup>1</sup> · S. Narayanan<sup>1</sup> · L. A. Kumaraswamidhas<sup>1,2</sup>

Received: 31 October 2018 / Accepted: 30 August 2019 / Published online: 25 September 2019  
© Shiraz University 2019

## Abstract

In the present study, the flow and aerodynamic features of a sharp trailing edged flat plate airfoil are systematically compared with NACA0012 airfoil. The studies are conducted for three different Reynolds numbers  $1.89 \times 10^5$ ,  $2.83 \times 10^5$  and  $3.78 \times 10^5$  and angles of attack  $20^\circ$ ,  $25^\circ$  and  $30^\circ$ . The present study shows that the occurrence of vortex shedding phenomena for the flat plate is substantially different from NACA0012 airfoil. Further, the re-attachment location of the shed vortices is closer to the trailing edge for the flat plate, whereas for NACA0012 airfoil it occurs at a certain distance upstream of the trailing edge. The NACA0012 airfoil generates higher lift coefficients at a higher Reynolds numbers of  $2.83 \times 10^5$  and  $3.78 \times 10^5$ , whereas for the flat plate it occurs at a lower Reynolds number of  $1.89 \times 10^5$ . The spectra of lift coefficient reveal that the amplitude of the primary shedding frequency dominates for the flat plate and NACA0012 airfoil at lower and higher Reynolds numbers of  $1.89 \times 10^5$  and  $3.78 \times 10^5$ , respectively, while it becomes almost same for an intermediate Reynolds number of  $2.83 \times 10^5$ . The present study reveals that the drag coefficient at high Reynolds number ( $3.78 \times 10^5$ ) is directly proportional to the initial merging point of the two shed vortices for both the flat plate and NACA0012 airfoil.

**Keywords** NACA0012 airfoil · Flat plate · Sharp trailing edge · Lift/drag coefficients

## List of Symbols

$c$	Chord length of the foil (m)
$c_d$	Coefficient of drag
$c_l$	Coefficient of lift
$c_p$	Coefficient of pressure
$f$	Frequency (Hz)
$p$	Pressure (Pascal)
$Re$	Reynolds number ( $\rho U c / \mu$ )
$St$	Strouhal number ( $fc/U$ )
$U$	Free stream velocity (m/s)
$\alpha$	Angle of attack (AOA) ( $^\circ$ )

## 1 Introduction

The airfoils find immense applications in marine engineering, aircrafts wings, fans, wind turbines blades, propellers, UAV (unmanned aerial vehicle), MAV (micro aerial vehicle), etc. and are highly demanding field of study in the present time. The aerodynamic performance of the foil can be easily augmented by simply changing its profile according to the application. It comprises consideration of lift/drag characteristics, shedding phenomena, stall characteristics, etc. The flow past foils at high angles of attack include several complex phenomena such as vortex formation and shedding, flow separation and lift/drag fluctuations in post-stall conditions. Researchers have been investigating the above-mentioned phenomena for the last several decades in flat plates and NACA airfoils, separately for understanding the vortex mechanisms in the near and far wake and their influence on aerodynamic coefficients. The present paper experimentally and numerically compares the complex flow phenomena and the corresponding aerodynamic characteristics of the flat plate having sharp trailing edged with 12% thick symmetric NACA airfoil having the same chord and span. Some of the pertinent researches of the flow over foils are mentioned in the following.

✉ S. Narayanan  
snarayan.1979@gmail.com; narayan@iitism.ac.in

<sup>1</sup> Department of Mechanical Engineering, Indian Institute of Technology (ISM), Dhanbad, Jharkhand 826004, India

<sup>2</sup> Department of Mining Machinery Engineering, Indian Institute of Technology (ISM), Dhanbad 826004, India

Chen and Fang (1996) studied the sharp-edged bevelled plates for the range of Reynolds numbers ( $Re$ ):  $3.5 \times 10^3$  to  $3.2 \times 10^4$  and angles of attack (AOA):  $0^\circ$  to  $90^\circ$ . They found that the Strouhal number depends on the  $Re$  values as a result of flow re-attachment for small AOA ( $0^\circ$  to  $5^\circ$ ), while it is independent of  $Re$  value due to intense flow separation at high AOA ( $10^\circ$  to  $90^\circ$ ).

Cleaver et al. (2013) compared the forces/flow fields associated with small-amplitude plunging oscillations of NACA0012 airfoil and flat plate at  $0^\circ$  as well as  $15^\circ$ , angles of attack for a Reynolds number of 10,000. They observed that at high Strouhal numbers, stable deflected jets experienced by the NACA airfoil generate high lift coefficients, while the deflected jets experienced by the plate generate oscillating lift coefficient. At  $15^\circ$  angle of attack, the flat plate shows an increase in lift coefficient up to a Strouhal number of 1; thereafter, it degrades, owing to the convection of the leading edge vortices from the suction surface.

Johnson et al. (2014) numerically investigated the effectiveness of immersed boundary method to capture the flow phenomena over NACA0012 airfoil for various incidence angles and Reynolds' numbers varying from  $5 \times 10^5$  to  $1.86 \times 10^6$ . They found that the results obtained with immersed boundary method match very well with the experimental ones.

Lam and Leung (2005) investigated the characteristics of shed vortex from flat plate for different AOA values  $20^\circ$ ,  $25^\circ$  and  $30^\circ$  at a fixed  $Re$  value of 5300. They observed a series of vortices shed from the leading/trailing edges alternately, in the wake. They also found that the peak vorticity level of the vortex shed from the trailing edge is higher as compared to vortex shed from the leading edge.

Lam and Wei (2010) investigated the flow features behind a flat plate for AOA values ranging from  $20^\circ$  to  $45^\circ$ . They observed the shedding of the two chains of vortices from the leading and trailing edges at a Reynolds number of  $2 \times 10^4$ , thus forming a vortex street behind the plate.

Lee and Kang (2000) studied the boundary-layer transition phenomena over two NACA0012 airfoils in tandem placed at zero-degree incidence for various Reynolds' numbers. They observed that as the two airfoils approach towards each other the length of the transition region increases. They also noticed maximum rms velocity for  $y^+$  ranging from 15 to 20.

Lin et al. (2013) numerically studied the effect of wavy surface on the aerodynamic characteristics of a NACA0012 airfoil. They observed noticeable change in pressure coefficient on the wavy airfoil as compared with the conventional NACA0012 airfoil. They also observed that the lift coefficient of wavy airfoil is 20% higher than the traditional NACA0012 airfoil in the post-stall region.

Mizoguchi and Itoh (2013) investigated the effects of aspect ratio (i.e. ( $L/c$ )) on the flow features of rectangular

wings at a fixed  $Re$  value of  $\sim 10^4$ . They found that the aerodynamic features were substantially affected by the separation bubbles from the leading edge at low Reynolds numbers for  $L/c > 3$ . Also, they observed considerable variations in the flow properties due to wing tip vortices for  $L/c < 3$ , as compared with the wings having large aspect ratios.

Kunihiko and Colonius (2009) numerically investigated flow over low-aspect-ratio flat plate at low Reynolds numbers (300–500) with the help of immersed boundary method. They observed that the aspect ratio and angles of attack play a vital role in the stability of the wake profile and aerodynamic forces.

Yang et al. (2012) investigated wake patterns with asymmetric behaviour behind a flat plate for the AOA values ( $20^\circ$ ,  $25^\circ$  and  $30^\circ$ ) at a fixed  $Re$  value of 1000. They noticed that the vortex shed from the trailing edge of an inclined plate has higher strength in comparison with that shed from the leading edge.

Narasimhamurthy and Andersson (2009) experimentally studied the aerodynamics of flapped airfoil at high AOA and compared their results with Leishman's model. They found that the results obtained from experiments matched well with Leishman's model at low amplitude but at high amplitude it showed large deviation from the Leishman's model.

Shehata et al. (2018) experimentally investigated NACA0012 airfoil pitching at different trajectories such as sinusoidal, trapezoidal, saw-tooth and reverse saw-tooth at a Reynolds number of  $2.1 \times 10^4$  and AOA in the range of  $3.5^\circ$ – $12^\circ$ . They observed that trapezoidal waveform provided higher gain in lift amplitude as compared to other waveforms studied.

Shehata et al. (2019) analytically and numerically investigated the aerodynamics load and frequency response of pitching NACA airfoil at sea level to understand its dynamic behaviour. They found that the amplitude of lift decreases for low and medium frequencies whereas it increases for high frequency.

Zakaria et al. (2017) numerically investigated the flow phenomena over an NACA0012 airfoil for AOA varying from  $0^\circ$  to  $40^\circ$  and at a Reynolds number of 79,900 using different turbulence models, namely SA model, modified SA model and Reynolds stress model (RSM). They found that the Reynolds stress model provided superior predictions of shedding from the leading as well as trailing edge over SA as well as modified SA models.

Zakaria et al. (2018) investigated the plunging airfoil for the range of angles of attack from  $0^\circ$  to  $65^\circ$  at a reduced frequencies ranging from 0.15 to 0.95 for a fixed Reynolds number of 80,000. They observed an increase in lift amplitude in the stall regime at a reduced frequency of 0.7. They also performed an optimization-based approach for representing time-dependent lift by a fourth-order dynamical system.

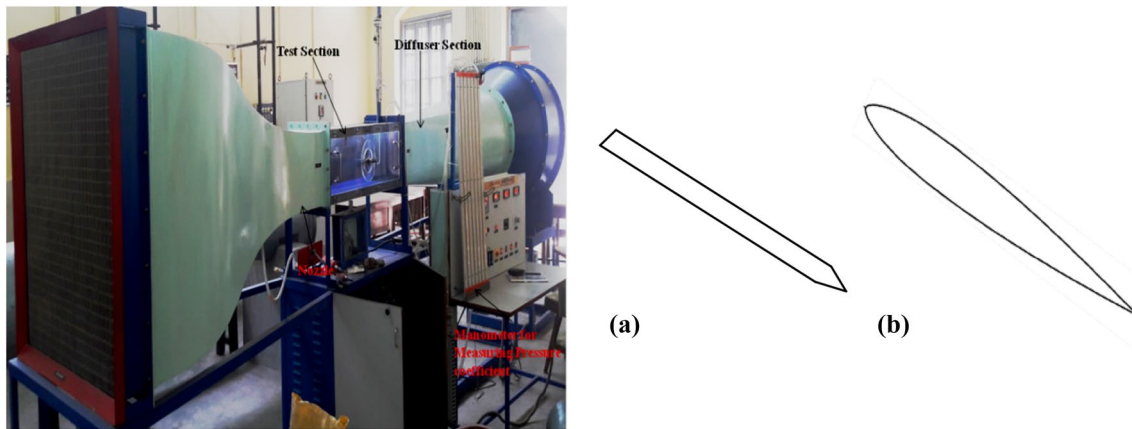


Fig. 1 Experimental set-up and schematics of **a** flat plate with sharp trailing edge and **b** NACA0012 airfoil

## 1.1 Objectives

In the past few decades, the detailed studies on the flow and aerodynamic characteristics of flat plate and NACA0012 airfoil have been investigated separately by a number of researchers but the detailed comparative study of the flow and aerodynamic characteristics of the flat plate with NACA0012 airfoil under the same parametric conditions is limited. Therefore, in the present study, the detailed numerical and experimental investigations on the flow and aerodynamic characteristics of the sharp trailing edged flat plate are compared with symmetric NACA airfoil having a maximum thickness to chord ratio of 12%. The comparisons of flow/aerodynamic characteristics between the sharp trailing edged flat plate and NACA0012 airfoil are made in terms of vortex shedding, spectra, near-wake and far-wake characteristics, lift and drag coefficients for three different chordwise  $Re$  values (i.e.  $1.89 \times 10^5$ ,  $2.83 \times 10^5$ ,  $3.78 \times 10^5$ ) at high angles of attack (i.e.  $20^\circ$ ,  $25^\circ$  and  $30^\circ$ ).

## 2 Experimental Set-Up and Numerical Methodology

### 2.1 Experimental Facility

The experiments were conducted in a subsonic open-circuit wind tunnel (Fig. 1) of the Fluid Flow Laboratory at IIT (ISM), Dhanbad. The main parts of the wind tunnel include: effuser with contraction ratio of 9:1, test section with dimensions of  $300 \text{ mm} \times 300 \text{ mm} \times 1000 \text{ mm}$  provided with transparent window on either side for visualizing complex flow features, blower unit with 12 blades fitted with a ten-HP, two-pole, three-phase AC motor. Three-component S-type load cell is used to measure the lift and drag forces, multi-tube manometer which contains 13 straight tubes for

measuring the static pressure at various locations of the object, placed in the test section. A smoke generator is used to generate homogeneous smoke over the foil, and the flow is visualized using a high-speed digital camera (model: IL5L and make: Fastech). A mesh screen is provided at the inlet of wind tunnel to reduce the turbulence levels in the tunnel and hence to obtain the smooth flow in the test section. The schematics of the sharp trailing edged flat plate and NACA0012 airfoil are shown in Fig. 1.

## 3 Numerical Techniques

### 3.1 Domain and Boundary Condition

The computational grid and boundary condition for the flow over flat plate and airfoil are chosen as same for unique comparison of flow and aerodynamic characteristics. The domain, boundary condition as well as grid for the present simulation are shown in Fig. 2. The size of the domain is restricted to  $35c$  in stream-wise direction and  $10c$  in the transverse direction for capturing the multifaceted flow features. The leading edge of the foil is placed at distance of  $7c$ , while the domain is extended up to  $28c$  from trailing edge so as to capture the multifaceted flow features in the near/far regions. The grid (Fig. 2) is constructed using a commercial CFD package ANSYS Workbench. The complex flow features over the NACA0012 airfoil and flat plate are predicted using ANSYS Fluent. Grids with approximately 20,000 to 140,000 cells are generated using commercial CFD package for different parameters. To resolve the boundary layer properly and hence to capture the complex flow features, fine mesh is used in the vicinity of the NACA0012 airfoil and flat plate surfaces and coarse mesh is provided far away from the body, where the flow effects are almost negligible.

**Fig. 2** Computational grid, domain and boundary condition

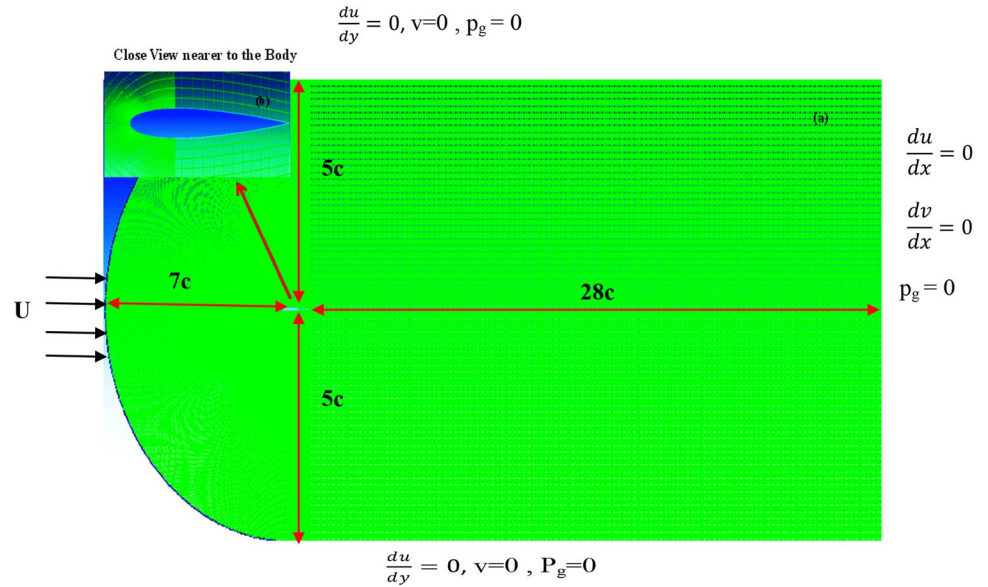
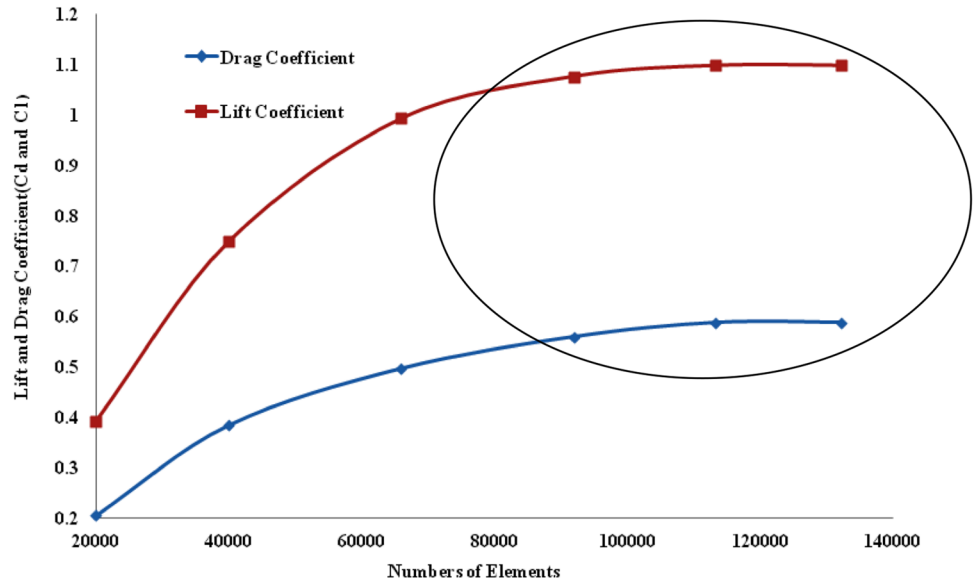


**Fig. 3** Variation of lifts and drag coefficient with number of grids



**3.2 Grid Independency Test and Turbulence Model**

The grid independence test is performed by varying the number of cells from 20,000 to 140,000. It is noticed that the lift and drag coefficients obtained with 100,009, 120,012 and 140,000 cells are almost invariant with further grid refinement (Fig. 3). The boundary layer formed over the foil is solved by restricting the highest wall  $y+$  value within 110. 2D unsteady numerical simulation is performed using commercial CFD package with a second-order pressure-based implicit solver, using SIMPLE algorithm. The current simulations are carried out using flow as incompressible with no-slip boundary condition imposed at the walls. The time step size for the present computation is chosen as  $3 \times 10^{-5}$

to predict the multifaceted features of flow such as vortex shedding, spectra, lift/drag and coefficients from the foil. The turbulence model and the governing equations for the present computation are given in Jha et al. (2019).

**3.3 Validation and Uncertainty Estimates**

The lift/drag, coefficients as well as the Strouhal number obtained from the present simulation given in Tables 1, 2 and 3 at  $45^\circ$  AOA were matched well with those obtained by Lam and Wei (2010). Further, the comparisons of pressure coefficients (Fig. 4) obtained from present computation for NACA0012 airfoil and flat plate also showed good agreement (i.e. within 8%), with those measured by Fage

**Table 1** Comparison of maximum drag coefficient obtained from present computation at 45° angle of attack with those predicted by Lam and Wei (2010), at the same parametric conditions

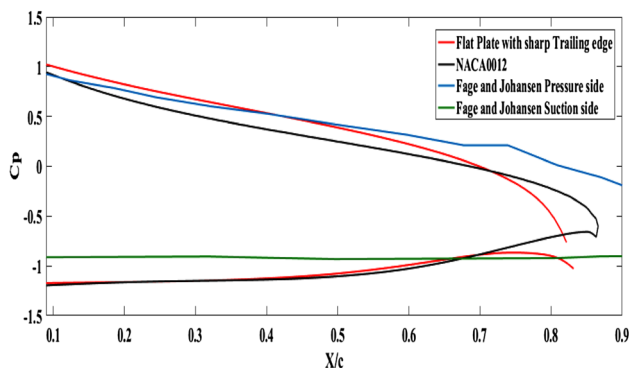
Maximum drag coefficient from present computation at 45° angle of attack	Maximum drag coefficient obtained for Lam and Wei (2010) for 45° angle of attack	% Deviation between Lam and Wei (2010) and present simulation
2.38	2.48	4.2016

**Table 2** Comparison of maximum lift coefficient obtained from present computation at 45° angle of attack with those predicted by Lam and Wei (2010), at the same parametric conditions

Maximum lift coefficient from present computation at 45° angle of attack	Maximum lift coefficient obtained for Lam and Wei (2010) at 45° angle of attack	% Deviation between Lam and Wei (2010) and present computation
2.39	2.47	3.34728

**Table 3** Comparison of fundamental frequency obtained from present simulation with those predicted by Lam and Wei (2010)

Strouhal number obtained from present computation at 45° angle of attack	Strouhal number obtained by Lam and Wei (2010) at 45° angle of attack,	% Deviation between Lam and Wei (2010) and present computation
0.225	0.23	2.22

**Fig. 4** Comparison of pressure coefficient for flat plate and NACA0012 airfoil at  $Re = 3.78 \times 10^5$  and 30° angle of attack

and Johansen (1927). The steady lift curve (Fig. 5) obtained from the simulation at a fixed  $Re$  value of  $3.78 \times 10^5$  showed good agreement with our own experimental results for both the flat plate and NACA0012 airfoil. The uncertainties in the experiments are estimated based on Moffat (1988). The uncertainties in the flow velocity and aerodynamic force measurements are within  $\pm 2\%$  and  $\pm 3\%$ , including repeatability

factors. The uncertainties in aerodynamic coefficients are well within  $\pm 2\%$ .

## 4 Results and Discussion

### 4.1 Vortex Shedding Mechanisms

The flow over a flat plate/NACA0012 airfoil at a Reynolds number of  $1.89 \times 10^5$  and 30° AOA obtained from current predictions is compared with flow visualization in Fig. 6. The flow features such as shed vortices from the edges and flow separation obtained from our predictions matched very well with those obtained using smoke-flow visualization, thus supporting the present simulation. The shedding mechanisms from the leading/trailing edges are explained in the following.

The comparison of stream lines of flat plate and NACA0012 airfoil at a fixed  $Re$  value of  $3.78 \times 10^5$  and 30° AOA is shown in Fig. 7 for various time instances from 0.6 to 0.7 s, to explain the flow/shedding mechanisms. The occurrence of shedding from the leading as well as trailing edges of the flat plate and NACA0012 airfoil plays an important role in modifying the aerodynamic features, and thus, it has to be studied in detail to understand the difference in the flow as well as shedding characteristics between the flat plate and NACA0012 airfoil. The shedding mechanisms from the sharp trailing edged plate and NACA0012 airfoil are explained in the following.

The flow separation occurs from the leading edge of both the flat plate and NACA0012 airfoil (Fig. 7a, b), and separated shear layer rolls up into a clockwise vortex, which grows in the stream-wise direction and re-attaches at a location very close to the trailing edge (i.e. 14 cm from the leading edge of the flat plate), while in NACA0012 airfoil the re-attachment point is ahead of the flat plate (i.e. 12 cm from leading edge of the airfoil), as shown in Fig. 7a. The counterclockwise vortex starts to form from the trailing edge (Fig. 7c) due to the migration of the flow from the high pressure surface to the low-pressure suction surface. The high suction pressure created by the growing clockwise vortex causes counterclockwise vortex near the trailing edge to grow in size (Fig. 7d) normal to the body and pushes the clockwise vortex towards the leading edge. The minimum lift is obtained as the counterclockwise vortex at the trailing edge attains a maximum size (Fig. 7e); thereafter, it sheds from the trailing edge of the flat plate/airfoil. The key difference in the vortex shedding features is that the size of the vortex shed from flat plate is higher than that of the airfoil. It indicates that the energy contained in the vortex shed from the flat plate is lower than the airfoil which further indicates that the maximum lift is lower in flat plate as compared to NACA airfoil (Table 4).

**Fig. 5** Steady lift versus angle of attack for **a** NACA0012 airfoil and **b** flat plate with sharp trailing edge at a Reynolds number of  $3.78 \times 10^5$

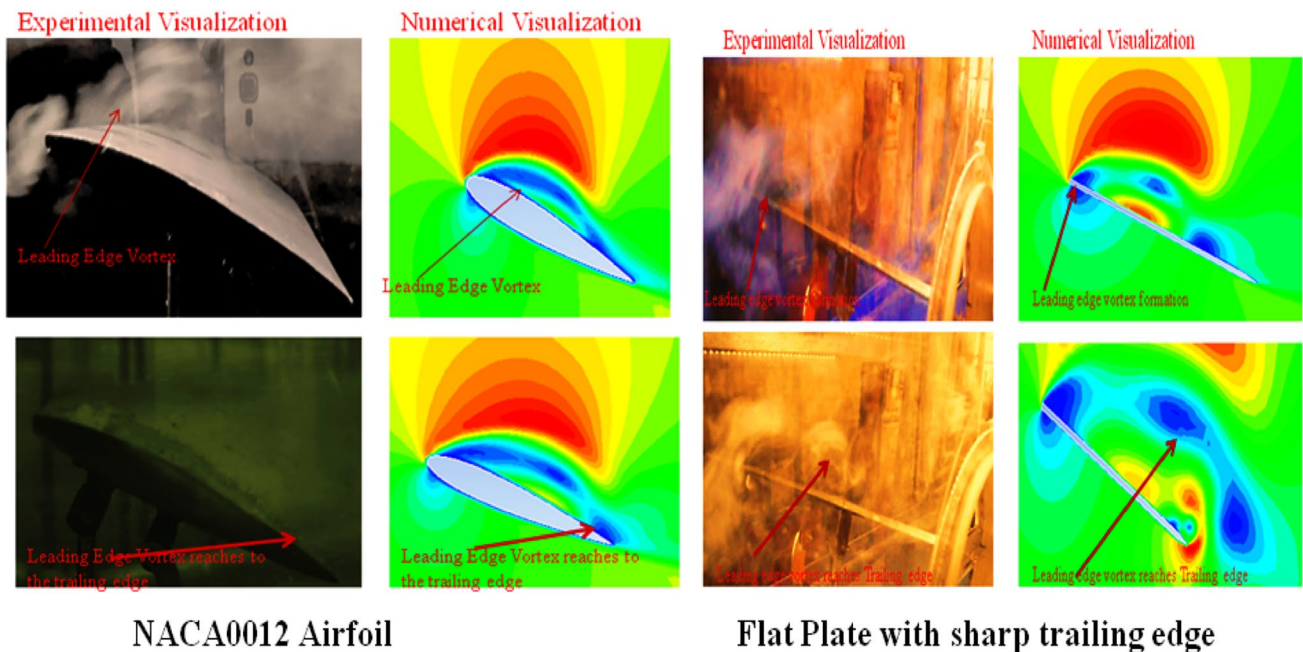
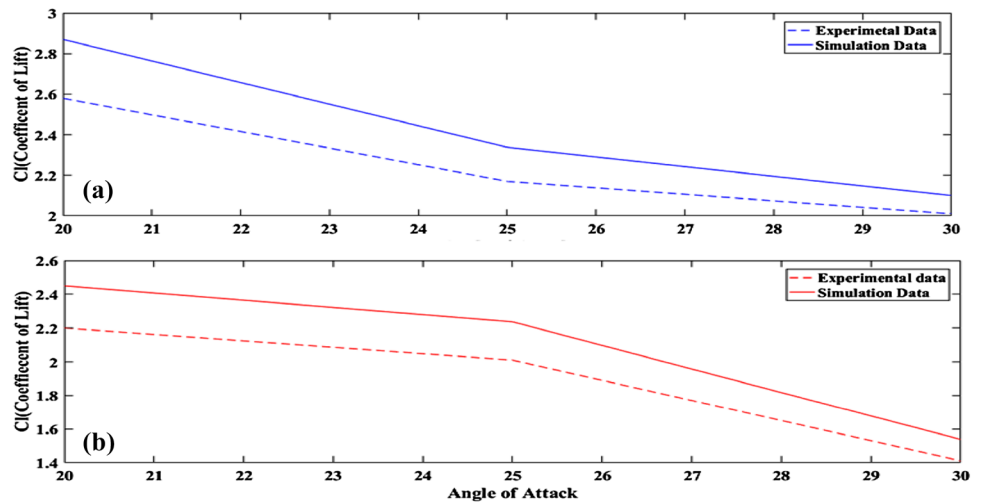


**Fig. 6** Comparison of smoke-flow visualization experiments over a flat plate and NACA0012 airfoil with present computation for  $30^\circ$  angle of attack at a Reynolds number of  $1.89 \times 10^5$

### 4.2 Lift/Drag Coefficients

The variations of lift/drag coefficients with normalized time for both NACA0012 airfoil and sharp trailing edged flat plate at  $30^\circ$  angle of attack for a Reynolds number of  $1.89 \times 10^5$  are shown in Fig. 8a. It is noticed that the lift/drag coefficients of the plate are 14% and 32%, higher than those of the NACA airfoil. Also, it is noticed that the lift/drag coefficients of the plate are out of phase with the NACA0012 airfoil. Lissajous figure shown in Fig. 8b, c reveals that the oscillations of lift and drag coefficients of the flat plate and NACA0012 airfoil are periodic and

in phase. The variations of lift/drag coefficients as well as its rms values (i.e.  $c_l'$  and  $c_d'$ ) obtained from the present computation are compared with those obtained from the experiments for different Reynolds numbers at  $30^\circ$  angle of attack (Tables 4, 5). It reveals that the NACA0012 airfoil generates higher lift and drag coefficients at higher Reynolds numbers as compared to the flat plate. The  $c_l'$  and  $c_d'$  show an increasing trend in NACA0012 airfoil, while in flat plate the  $c_l'$  first increases and then decreases but negligible variation is noticed in  $c_d'$  with an increase in Reynolds number. Further, it is observed that the Strouhal number shows a decreasing behaviour with

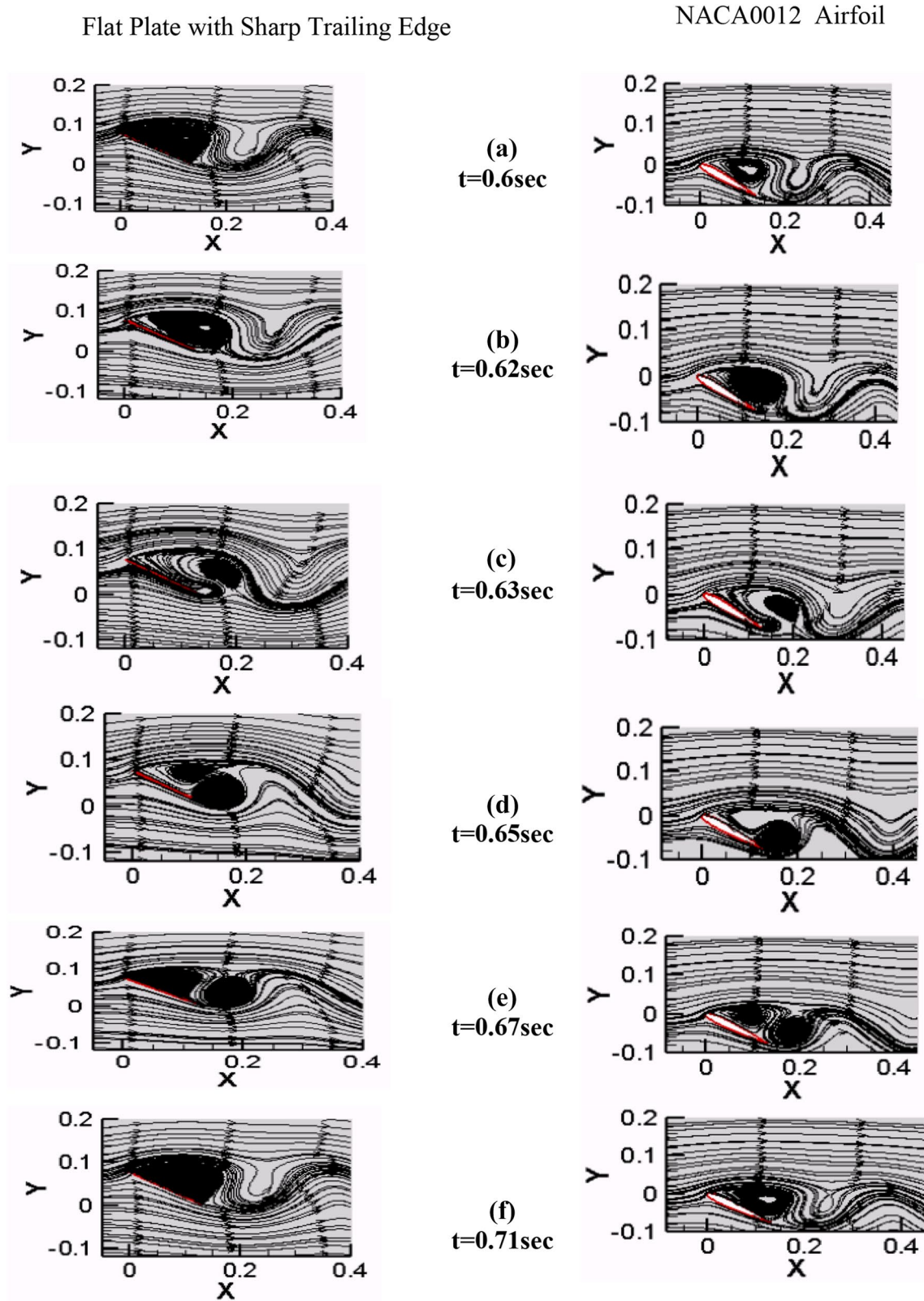


**Fig. 7** Comparison of stream lines for flow over **a** NACA0012 airfoil and **b** flat plate, at  $Re = 3.78 \times 10^5$  and  $30^\circ$  angle of attack for different time instances

**Table 4** Computed lift coefficient characteristics of flow over a flat plate and NACA0012 airfoil for different Reynolds numbers at 30° angle of attack

$Re. no. \times 10^5$	$\alpha$ (°)	$c_l$ (flat plate)			Error (%)	$c_l$ (NACA0012)			Error (%)
		Experimental	Numerical	$c_{l_{rms}}$		Experimental	Numerical	$c_{l_{rms}}$	
1.89	30	1.5235	1.3515	0.0931	11.2897	1.2894	1.1546	0.0673	10.45
2.83	30	1.5412	1.3631	0.1156	11.5559	1.3213	1.1722	0.0691	11.28
3.78	30	1.5376	1.3617	0.0953	11.4399	1.9846	2.0998	0.1241	5.59

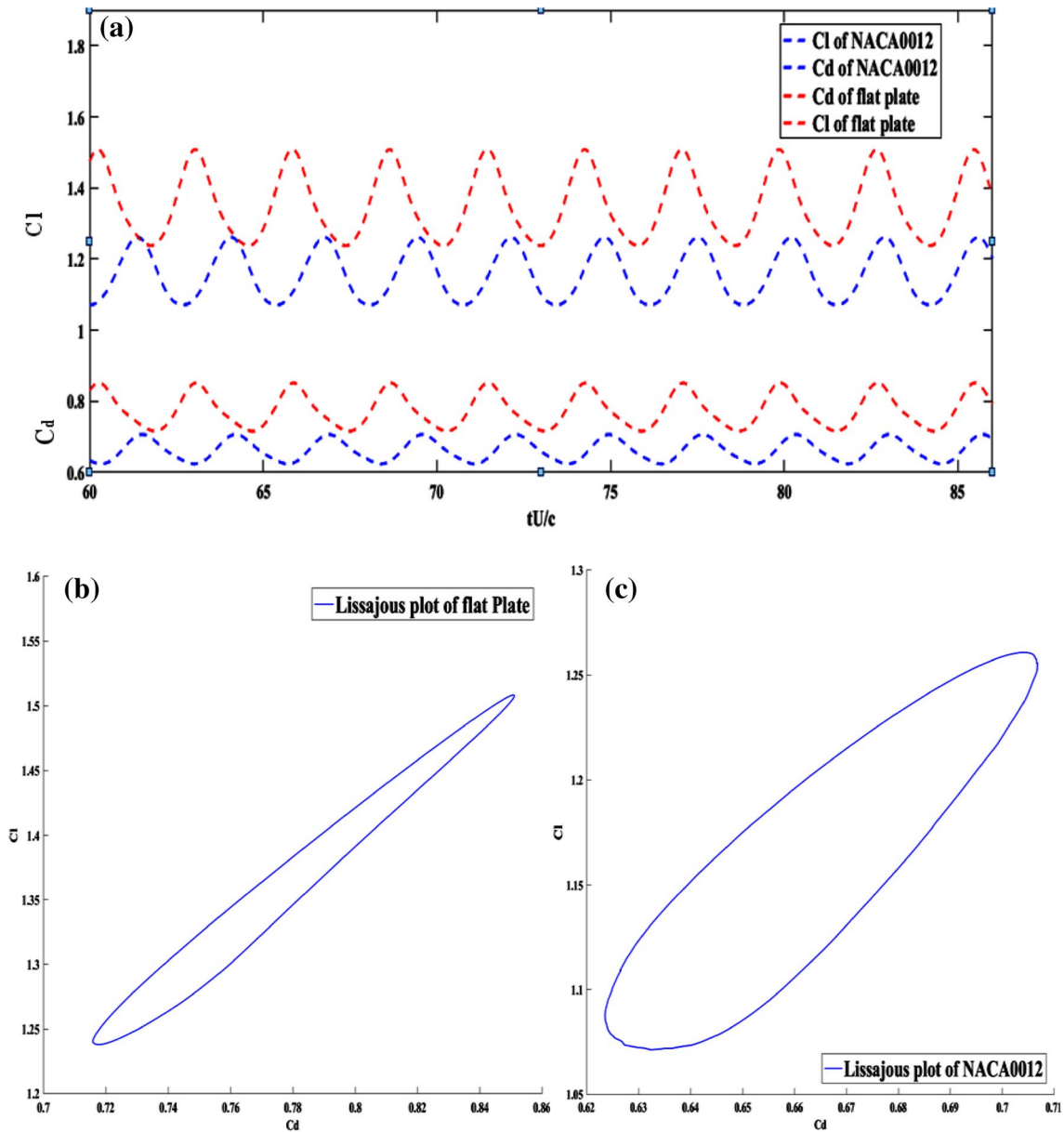


**Fig. 8** Comparison of  $c_l$ ,  $c_d$  and Lissajous plots for NACA0012 airfoil and flat plate at  $Re = 2.83 \times 10^5$  and 30° angle of attack



**Table 5** Computed drag coefficient characteristics of flow over a flat plate and NACA0012 airfoil for different Reynolds numbers at 30° angle of attack

$Re. no. \times 10^5$	$\alpha$ (°)	$c_d$ (flat plate)			Error (%)	$c_d$ (NACA0012)			Error (%)
		Experimental	Numerical	$C_{drms}$		Experimental	Numerical	$C_{drms}$	
1.89	30	0.8319	0.7743	0.0455	6.9239	0.7125	0.6618	0.0284	7.12
2.83	30	0.8362	0.7779	0.0464	6.9720	0.7312	0.6679	0.0295	8.66
3.78	30	0.8471	0.7786	0.0467	8.0864	1.0829	1.1929	0.0531	9.22

**Table 6** Variation of  $St$  no with angle of attack and Reynolds number for flat plate and NACA0012 airfoil

$Re. no \times 10^5$	$St. no. for flat plate$			$St. no. for NACA0012$		
	20°	25°	30°	20°	25°	30°
1.89	0.5212	0.4149	0.3517	0.4827	0.4759	0.3746
2.83	0.5115	0.4209	0.3608	0.4801	0.4727	0.3739
3.78	0.5099	0.4239	0.3585	0.4794	0.4683	0.3777

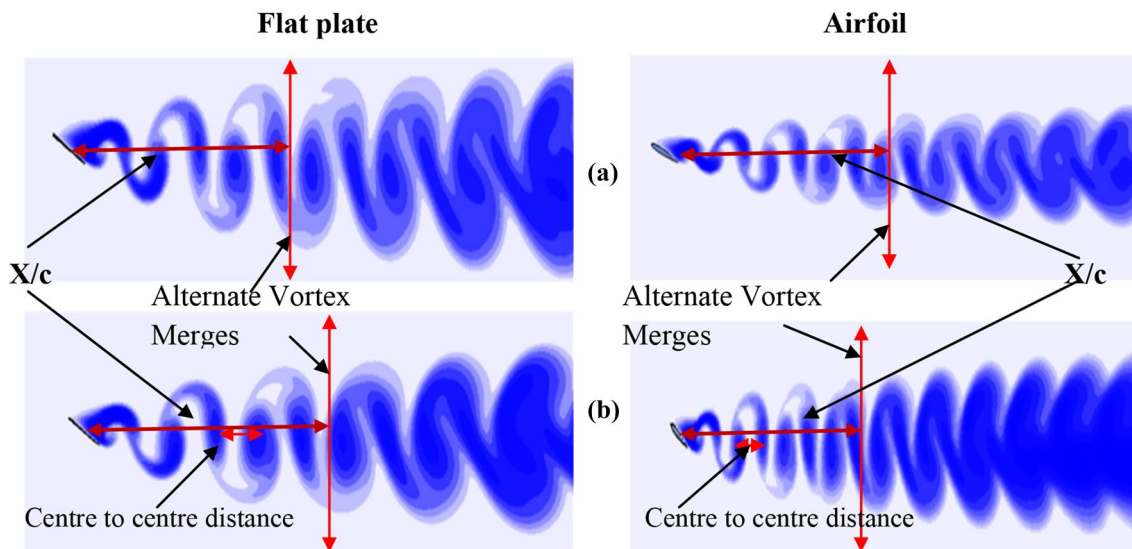


**Fig. 9** Comparison of instantaneous stream-wise vorticity contours at 0.8 s for flat plate and NACA0012 airfoil for three different angles of attack **a** 25° and **b** 30°, at a Reynolds number of  $3.78 \times 10^5$

an increase in angles of attack for both the flat plate and NACA0012 airfoil at all the Reynolds numbers studied (Table 6).

### 4.3 Instantaneous Vorticity Contours

Instantaneous stream-wise vorticity contours of flat plate and NACA0012 airfoil are shown in Fig. 9 (i.e. 0.5 s) for different AOA at a Reynolds number of  $1.89 \times 10^5$ . In general, it is seen that vortex shed from the flat plate is larger than NACA0012 airfoil for all the  $Re$  values studied. At high angles of attack (i.e. 25° and 30°) strong vortex shedding is observed from both the leading and trailing edges for both the flat plate and NACA airfoil.

Even though the vortex shedding pattern from flat plate and NACA0012 airfoil is almost same, but the centre-to-centre distance between the subsequent shed vortices is higher in flat plate as compared to the NACA airfoil. The two alternately shedding vortices extending up to a normalized stream-wise distance (i.e.  $x/c < 7$ ) is seen in the near-wake zone, for both the flat plate and NACA0012 airfoil. In flat plate, the two alternately shedding vortices merge at a certain  $x/c$  value in the near-wake zone and generate a low drag coefficient since the merging point is closer to the trailing edge while in NACA0012 airfoil large drag coefficient is observed since the merging of two alternately shed vortices occurs at some distance higher than that observed in flat plate. Thus, the

**Fig. 10** Velocity contour plot of **a** flat plate and **b** NACA0012 airfoil showing the near- and far-wake zone

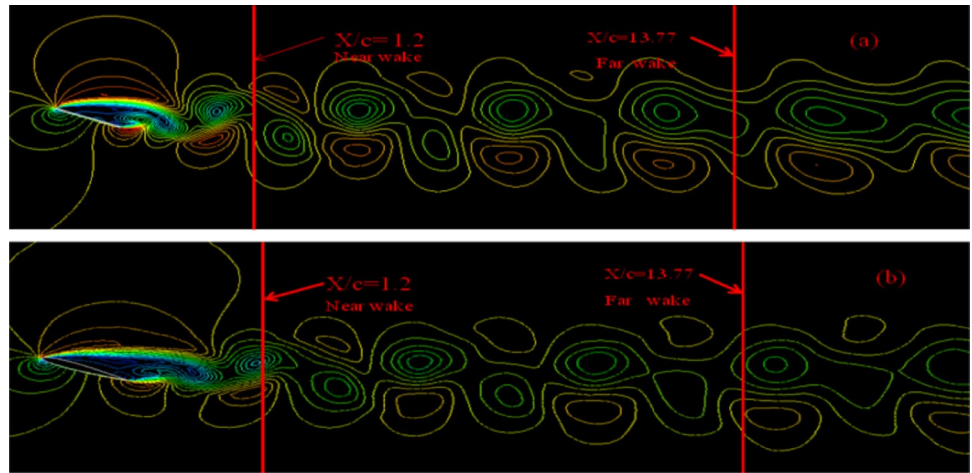
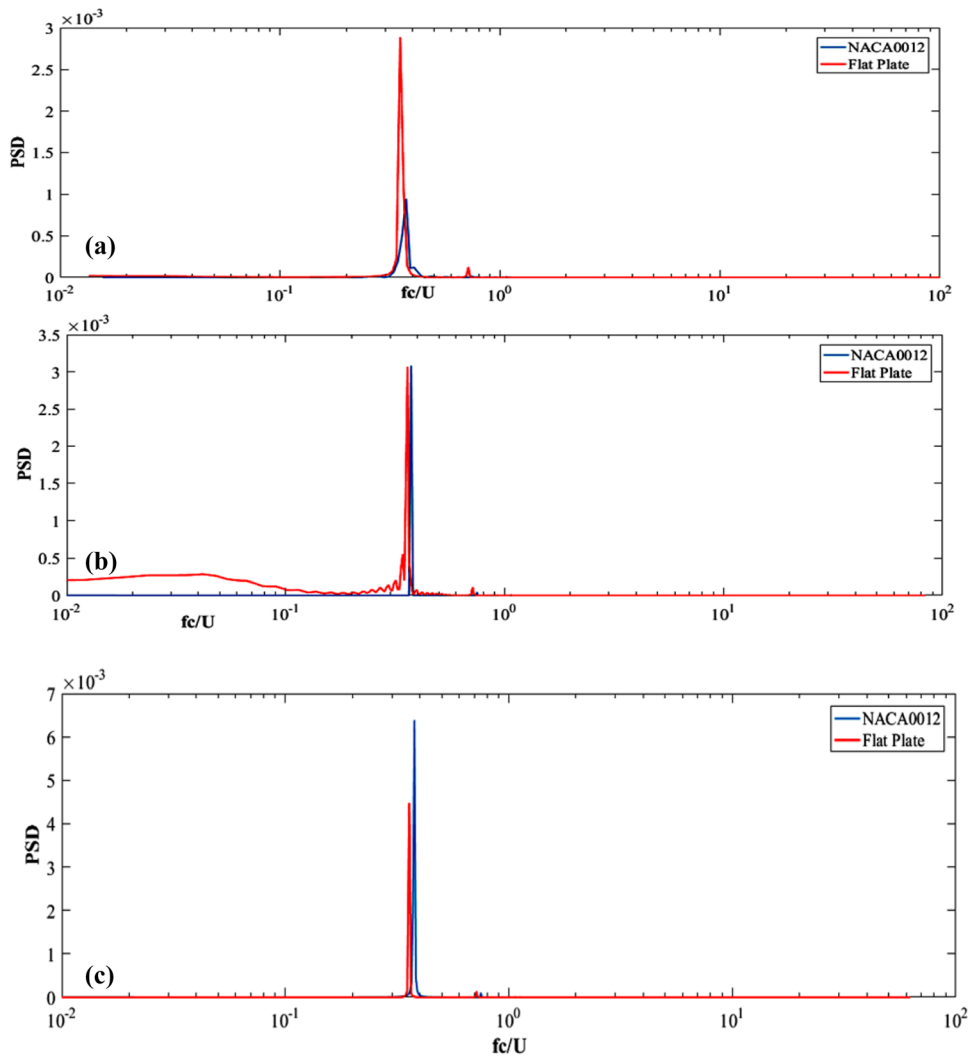


**Fig. 11** Comparison of lift coefficient spectra with Strouhal number for NACA0012 airfoil and flat plate at different Reynolds numbers **a**  $1.89 \times 10^5$ , **b**  $2.83 \times 10^5$  and **c**  $3.78 \times 10^5$



present study shows that the drag coefficient is directly proportional to the merging point of the two alternatively shed vortices in both the flat plate and NACA0012 airfoil (Fig. 9).

#### 4.4 Wake Characteristics

The near-wake region is observed up to normalized distance  $x/c$  of 7 in stream-wise direction while far-wake region begins beyond an  $x/c$  value of 13.77 (Jha et al. 2019) as shown in Fig. 10, from the trailing edge for both the foils. To understand near-wake oscillation phenomena of the vortices shed from NACA0012 airfoil and sharp trailing edged flat plate, the power spectral density (PSD) of stream-wise velocity components at an  $x/c$  of 1.4 for different  $Re$  values  $1.89 \times 10^5$ ,  $2.83 \times 10^5$  and  $3.78 \times 10^5$  at  $30^\circ$  angle of attack is shown in Fig. 11. The sampling rate of velocity time series is kept as 33 kSa/s (i.e.  $1/3 \times 10^{-5}$  s) for all  $Re$  values ( $1.89 \times 10^5$ ,  $2.83 \times 10^5$  and  $3.78 \times 10^5$ ), and the frequency resolution of computed spectra is 1.62 Hz. The spectra of the near-wake showed only single peak for all the  $Re$  studied, which corresponds Karman frequency,  $St_p$ . It is also observed that the small-scale near-wake structure fluctuates at high frequency (Fig. 11). Further, the spectra of the stream-wise velocity components reveal that the amplitude of the Karman shedding frequency dominates for the flat plate at a lower  $Re$  value of  $1.89 \times 10^5$  but it dominates for NACA0012 airfoil at a higher  $Re$  value of  $3.78 \times 10^5$ , whereas it becomes almost same for an intermediate  $Re$  value of  $2.83 \times 10^5$ . The generation of high lift coefficient

in NACA0012 airfoil at high  $Re$  value may be due to the increase in the energy contained in the near-wake vortices as compared to the flat plate.

The velocity spectra at a stream-wise distance ( $x/c$ ) of 14 (i.e. far-wake zone) for different  $Re$  values:  $1.89 \times 10^5$ ,  $2.83 \times 10^5$  and  $3.78 \times 10^5$ , at  $30^\circ$  angle of attack are shown in Fig. 12, for both the flat plate and NACA0012 airfoil. The far-wake PSD reveals the presence of secondary frequency due to complex nonlinear interaction of the vortices shed from the plate and NACA0012 airfoil for all the  $Re$  values studied. The spectra show that the amplitude of the secondary undulations is dominant for the NACA0012 airfoil at a low  $Re$  value of  $1.89 \times 10^5$  whereas it dominates for flat plate at an intermediate  $Re$  value of  $2.83 \times 10^5$ . Further, at high  $Re$  of  $3.78 \times 10^5$  the presence of multiple frequencies is observed in the spectra, which may be due to the further undulations of the secondary vortices.

#### 5 Conclusions

The flow past a sharp trailing edged flat plate and NACA0012 airfoil was systematically compared in the present study to understand the complex flow phenomena occurring in the zones,  $x/c < 7$  (i.e. near wake) and  $x/c > 7$  (i.e. far wake), and its influence on the aerodynamic properties (lift, drag) for various  $Re$  values at high angles of attack. The comparisons of sharp trailing edged plate and NACA0012, placed at high angles of attack, are made using streamlines, instantaneous vorticity contours, near- and

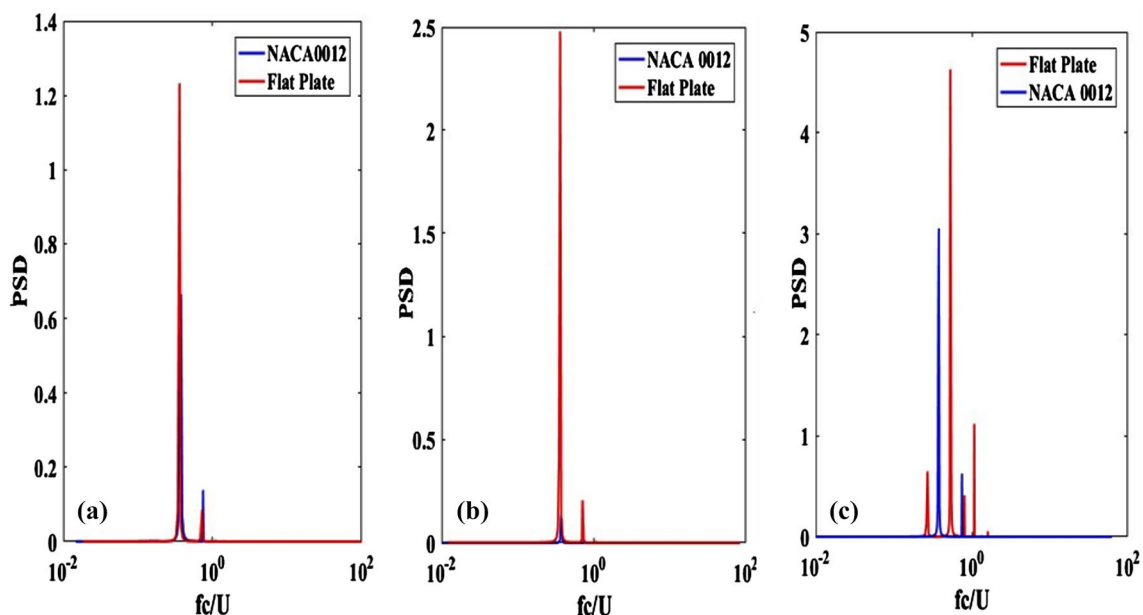


**Fig. 12** Comparison of velocity fluctuation spectra in the far-wake region with Strouhal number at different Reynolds numbers, **a**  $1.89 \times 10^5$ , **b**  $2.83 \times 10^5$  and **c**  $3.78 \times 10^5$

far-wake spectra, etc. The streamlines clearly depict that the size of the shed vortex from plate is higher than from NACA0012 airfoil at high  $Re$  value. The energy of the vortex shed from the plate is lower as compared to the NACA0012 airfoil. Thus, it illustrates that the NACA0012 airfoil generates high lift coefficient in comparison with the flat plate at high  $Re$  value. It is noticed that the unsteady drag and lift coefficients of the flat plate and NACA0012 airfoil are out of phase, thus following a periodically repeating behaviour. Further, it is noticed that the unsteady lift and drag coefficients of flat plate and NACA0012 airfoil are in phase, when compared separately. The Lissajous plots reveal that the unsteady drag and lift coefficients oscillate at the same frequency, for both the plate and NACA0012 airfoil. The stream-wise vorticity contours shown at high Reynolds number reveal that the drag coefficient is directly proportional to the initial merging point of the shed vortices for both the flat plate and NACA0012 airfoil. The spectra of stream-wise velocity components for the flat plate and NACA0012 airfoil show the presence of Karman vortices in the near-wake zone with single frequency while in the far wake it shows two dominant frequencies corresponding to Karman shedding/secondary large-scale oscillations. Thus, the present study sufficiently demonstrates the difference in the flow/shedding behaviours of a flat plate with NACA0012 airfoil.

**Acknowledgements** The authors gratefully acknowledge that the current work (ECR/2016/000640) has been supported by DST (Science and Engineering Research Board (SERB)).

## References

- Chen JM, Fang Y-C (1996) Strouhal numbers of inclined flat plates. *J Wind Eng Ind Aerodyn* 61(2-3):99–112
- Cleaver DJ, Wang Z, Gursul I (2013) Investigation of high-lift mechanisms for a flat-plate airfoil undergoing small-amplitude plunging oscillations. *AIAA J* 51(4):968–980
- Fage A, Johansen FC (1927) On the flow of air behind an inclined flat plate of infinite span. *Proc R Soc Lond Ser A Contain Pap Math Phys Character* 116(773):170–197
- Jha SK, Narayanan S, Kumaraswamidhas LA (2019) Investigations of flow phenomena behind a flat plate with circular trailing edge. *J Braz Soc Mech Sci Eng* 41(5):227
- Johnson JP, Iaccarino G, Chen K-H, Khalighi B (2014) Simulations of high Reynolds number air flow over the NACA-0012 airfoil using the immersed boundary method. *J Fluids Eng* 136(4):040901
- Kunihiko T, Colonius T (2009) Effect of tip vortices in low-Reynolds-number poststall flow control. *AIAA J* 47(3):749–756
- Lam KM, Leung MYH (2005) Asymmetric vortex shedding flow past an inclined flat plate at high incidence. *Eur J Mech B Fluids* 24(1):33–48
- Lam KM, Wei CT (2010) Numerical simulation of vortex shedding from an inclined flat plate. *Eng Appl Comput Fluid Mech* 4(4):569–579
- Lee H, Kang S-H (2000) Flow characteristics of transitional boundary layers on an airfoil in wakes. *J Fluids Eng* 122(3):522–532
- Lin YF, Lam K, Zou L, Liu Y (2013) Numerical study of flows past airfoils with wavy surfaces. *J Fluids Struct* 36:136–148
- Mizoguchi M, Itoh H (2013) Effect of facet ratio on aerodynamic characteristics at low Reynolds numbers. *AIAA J* 51(7):1631–1639
- Moffat RJ (1988) Describing the uncertainties in experimental results. *Exp Therm Fluid Sci* 1(1):3–17
- Narasimhamurthy VD, Andersson HI (2009) Numerical simulation of the turbulent wake behind a normal flat plate. *Int J Heat Fluid Flow* 30(6):1037–1043
- Shehata H et al (2018) Aerodynamic analysis of flapped airfoil at high angles of attack. 2018 AIAA aerospace sciences meeting
- Shehata H et al (2019) Aerodynamic response of a NACA-0012 airfoil undergoing non-sinusoidal pitching waveforms. AIAA Scitech 2019 forum
- Yang D et al (2012) Three-dimensional wake transition behind an inclined flat plate a. *Phys Fluids* 24(9):094107
- Zakaria MY, Taha HE, Hajj MR (2017) Measurement and modeling of lift enhancement on plunging airfoils: a frequency response approach. *J Fluids Struct* 69:187–208
- Zakaria MY et al (2018) A computational study of vortex shedding from a NACA-0012 airfoil at high angles of attack. *Int J Aerodyn* 6(1):1–17